Highly Emissive Layers based on Organic/Inorganic Nanohybrids Using Aggregation Induced Emission Effect

Jonathan Phelipot, Nicolas Ledos, Thomas Dombray, Matthew P. Duffy, Mathieu Denis, Ting Wang, Yahia Didane, Meriem Gaceur, Qinye Bao, Xianjie Liu, Mats Fahlman, Pietro Delugas, Alessandro Mattoni, Denis Tondelier, Bernard Geffroy, Pierre-Antoine Bouit, Olivier Margeat, Jörg Ackermann, and Muriel Hissler**

J. Phelipot, T. Wang, Y. Didane, M. Gaceur, O. Margeat, J. Ackermann Aix Marseille Univ
CNRS
CINaM

Marseille, France
E-mail: olivier.margeat@univ-amu.fr

N. Ledos, T. Dombray, M. P. Duffy, M. Denis, P.-A. Bouit, M. Hissler Univ Rennes
CNRS
ISCR – UMR 6226, Rennes F-35000, France

E-mail: muriel.hissler@univ-rennes1.fr

Q. Bao, X. Liu, M. Fahlman Laboratory for Organic Electronics ITN
Linköping University
Norrköping, Sweden

The ORCID identification number(s) for the author(s) of this article can be found under https://doi.org/10.1002/admt.202100876.

P. Delugas, A. Mattoni
Istituto Officina dei Materiali (CNR – IOM) Cagliari
Cittadella Universitaria, Monserrato (Ca) I-09042, Italy
D. Tondelier, B. Geffroy
Laboratoire de Physique des Interfaces et des Couches Minces (LPICM) CNRS
Ecole Polytechnique, IP Paris, Palaiseau Cedex, France
B. Geffroy
Université Paris-Saclay
CEA
CNRS
NIMBE
LICSEN
Gif-sur-Yvette 91191, France

DOI: 10.1002/admt.202100876
Adv. Mater. Technol. **2021**, 2100876

Fluorescent nanohybrids, based on π-extended hydroxyoxophosphole ligands grafted onto ZnO nanoparticles, are designed and studied. The restriction of the intramolecular motions of the organic fluorophore, through either aggregates' formation in solution or processing into thin films, forms highly emissive materials due to a strong aggregation induced emission effect. Theoretical calculations and XPS analyses were performed to analyze the interactions between the organic and inorganic counterparts. Preliminary results on the use of these nanohybrids as solution-processed emissive layers in organic light emitting diodes (OLEDs) illustrate their potential for lighting applications.

1. Introduction

Light-emitting materials are nowadays important components in a large field of applications such as light-emitting diodes (LEDs),[1] security,[1] biology,[2] and nanomedicine.[3] For many applications, generation of highly emissive nanoparticles has opened new opportunities for future technologies such as QD- LEDs, lasers and bio-labeling.[4–6] Nano- and microscale materials with tailored emission properties have been developed with rationally designed organic molecules.[7–9] While these organic nanoparticles show strong emission, control over size, shape, distribution, and processing remains challenging.[7–9]

One possibility to enhance the emission of organic fluorophores and to control the size of emissive nanoparticles at the same time is their grafting onto inorganic nano- particle surfaces. For example, the cou- pling of fluorophore molecules with the plasmon resonance of metallic nanopar- ticles could enhance their emission.[10,11] Electronic interaction between the ligand molecule and the inorganic nanocore was found to form new emissive excited states of the ligands.[12] Thus, fluorescent nanohybrids are a fascinating new class of materials generating new or improved optical properties in a synergetic way from

both organic ligand and inorganic nanoparticles. However, in the objective of generating highly emissive hybrid nanoparti- cles, the grafting of organic ligands onto inorganic nanoparticle surfaces often to poor emission enhancement.[13] Indeed, many planar organic luminogens tend to aggregate due to strong π–π interaction, which usually turns off light emission. As a result, high concentration of ligands on the nanoparticle sur- face, needed to generate strong light emission, leads to aggre- gation-caused quenching phenomena (ACQ).[14,15] To prevent such quenching, molecular design offers a very elegant strategy to avoid detrimental intermolecular interaction and generates the contrary effect of ACQ, which refers to aggregation-induced emission (AIE) processes.[14] Once the molecules form aggre- gates, for example in thin films or in a crystal, strong fluores- cence enhancement is observed, due to the restriction of their intramolecular rotations in the aggregate state.[14] The AIE phenomenon is often based on the use of nonplanar propeller- shaped rotor-like structures. Such simplified picture works nicely with propeller-like derivatives such polyphenyl-siloles, phospholes, or tetraphenylethyelene. However, the photo- physics of solid-state luminophore is more complex than this simple AIE/ACQ duality.[16,17] Recently, a salicylaldehyde azine has been grafted onto colloidal $GaOOH/H_2O$ nanocubes,[18] generating strong hydrophobic interactions, which effectively restrict the molecular motions and thus enhance the emission. Similar trends were observed with carbazole derivatives on various inorganic or metal nanocrystals.[19,20] However, to be used in optoelectronic devices as an emitting layer, such organic–inorganic nanohybrid materials should provide suitable trans- port properties together with their optical emission, and be able to form thin films with optical quality. We thus envisaged to achieve such properties by using AIE ligands synergistically combined with semiconducting nanoparticles. In this work, we present the synthesis of AIE nanohybrids prepared via grafting organic AIE ligands onto high bandgap semiconducting nanoparticles. Zinc oxide (ZnO) was chosen as the inorganic material for both its ability to be easily functionalized and its potential electron transport properties as n-type semicon- ductor. Among the AIE fluorophores, we selected phosphole- based luminophores.[21–27] Hence, the phosphole stator allows accessing easily to hydroxyoxophosphole which can coordinate intimately onto metal oxide semiconductors.[28] The structure- properties relationships leading to highly emissive materials have been investigated. Integration of these novel nanohybrids into solution-processed LED demonstrates that this strategy allows generating electroluminescent films.

2. Results and Discussion

2.1. Nanohybrid Syntheses and Characterizations of the Grafting

The AIE nanohybrids were synthesized in solution by mole- cular grafting on the surface of ZnO nanospheres (diameter ≈ 6 nm) of one of the selected AIE ligands **1–3** (**Figure 1**a).[29,30] In a typical synthesis in organic solvents such as chloroform, a solution containing a specific amount of ZnO nanoparticles is mixed with a solution containing an adequate concentration of one of the AIE ligands allowing to control the amount of grafted molecules per ZnO nanoparticle. Varying the concentra- tion of ligands by keeping the amount of ZnO NPs constant is then used to produce AIE nanohybrids with different ratio of organic/inorganic composition. The scheme on Figure 1c rep- resents the nanohybrid formation in solution and the resulting emissive materials, either aggregates in solution or thin film when spin-coated on a substrate.

The efficient grafting of the ligands **1**, **2**, **3** via the hydroxy- oxophosphole group onto ZnO nanospheres was investigated by FTIR spectroscopy, XPS, and theoretical calculations. The powder FTIR spectra of compounds **2**, ZnO and nanohybrids ZnO:**2** (recovered from solution by centrifugation) clearly demonstrates the occurrence of the grafting (**Figure 2**a). It can be seen that

the band at 990 cm^{-1} corresponding to the γ(POH) vibration of compound **2** disappears after grafting as expected,[28,31] together with the removal of acetates from the ZnO surface (lower intensities for bands at 1440 and 1560 cm^{-1}),[32] while a new band at 1110 cm^{-1} appears that can be addressed to the γ(OPO) vibration.[28,33]

Theoretical calculations were realized by density func- tional theory (DFT) to study the different possible binding modes of **2** onto ZnO surfaces (see ESI for computational details). We focused in particular on the binding mode of

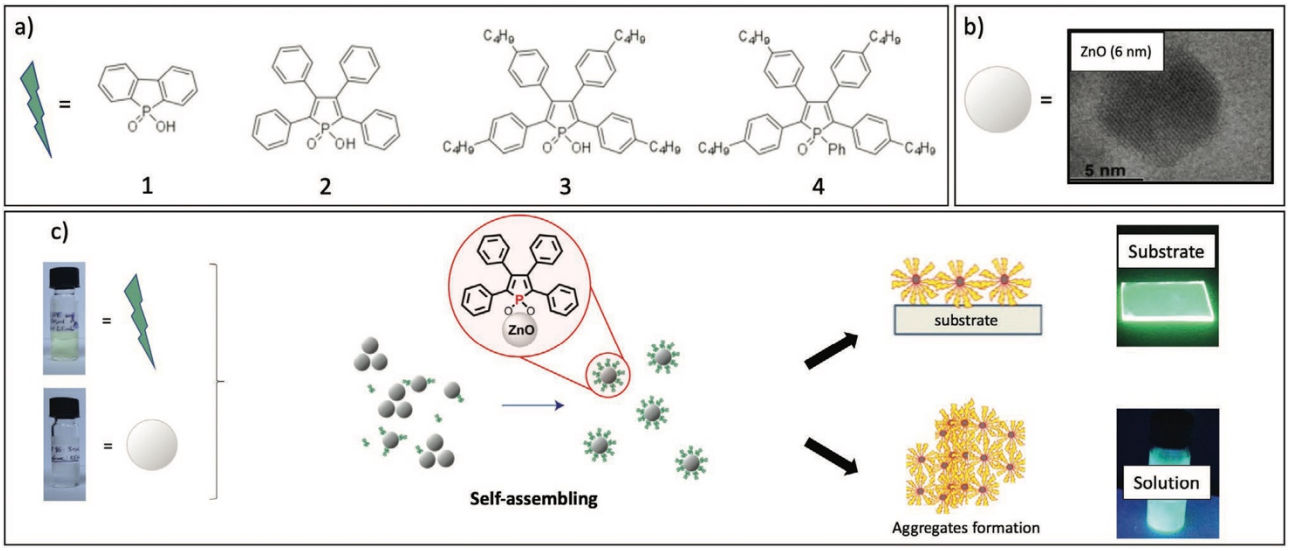

Figure 1. a) Molecular structures of the fluorescent molecules (**1**, **2**, **3**) bearing phosphole unit to bind to ZnO surface; molecule **4** is a reference phosp- hole without grafting unit. b) Zinc oxide nanoparticles used for the study. c) Scheme of the aggregation-induced emission (AIE) effect when molecules are grafted onto ZnO nanoparticles forming highly emissive materials, used as layer on a substrate or aggregates in solution.

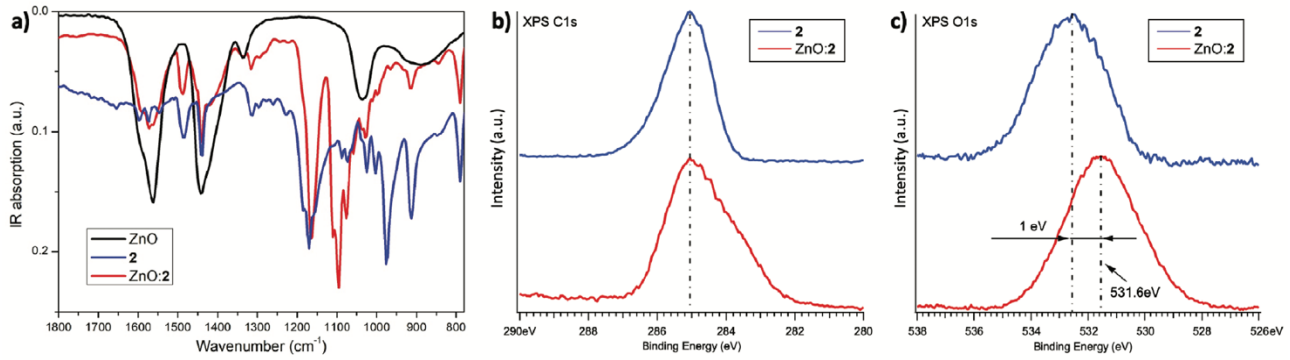

Figure 2. a) FTIR spectra of compounds **2**, ZnO and ZnO:**2**. b,c) XPS spectra of compounds **2** and ZnO:**2**.

hydroxyoxophosphole group exploring its bidentate, monoden- tate, protonated, and deprotonated configurations. The results clearly indicate that the bidentate grafting mode is the most stable configuration for the binding of **2** onto the ZnO surface, with the proton spontaneously moving from the POOH group to the surface. The band alignment in the case of **2** bonded on the nonpolar (01-10) crystalline ZnO surface has been cal- culated (Figure S4, Supporting Information). A downshift of the molecular levels is found with a weak charge displacement only visible at the O-Zn bond. Furthermore, the XPS analyses suggest the occurrence of charge transfer from the ZnO to the ligand **2** during grafting as a more electron rich environment in the molecule produces a shift toward lower binding energy in the XPS core level spectra. In details, the XPS analysis of nanohybrids ZnO:**2** as well as of the nongrafted ligand **2** show a new shoulder for C1s peak at lower binding energy after grafting (Figure 2b,c, and wide scan on Figure S5, Supporting Information). This shift is most likely due to charge transfer from the ZnO nanoparticle surface to carbon atoms. We fur- ther observe a shift toward lower binding energy for O1s, though this shift can be addressed to the contribution from the ZnO oxygens.[34]

2.2. Optical Properties of Nanohybrids in Solution

The absorption and emission spectra of the molecules **1**–**4** before and after adding ZnO in the chloroform solution were studied. Table S2 (Supporting Information) summarizes the optical parameters of the ligands. The ligands **2**–**4** exhibit □–□* absorption band centered around 380–410 nm in the UV-vis- ible region (**Figure 3** and Figure S6, Supporting Information), which is blue-shifted down to 280 nm for ligand **1** (Figure S7, Supporting Information). As anticipated, compounds **2**–**4** pre- sent a very weak emission in solution centered around 500–530 nm while compound **1**, as expected from its planar structure, dis- plays in solution a higher emission at 360 nm (see Table S2, Supporting Information). Then, the effects of their grafting on ZnO nanoparticles on the optical properties have been inves- tigated. When the concentration of ZnO nanoparticles was increased (monitored by UV absorption – Figure S7b, Sup- porting Information) in a chloroform solution of **1**, a severe quenching of the characteristic emission of the ligand was observed (Figure S7c, Supporting Information). The grafting of **1** onto ZnO nanoparticles leads indeed to strong ACQ effect due to the □–□ stacking at the ZnO surface.[35] Then finally, by continuing the addition of ZnO, the classical ZnO defect emis- sion at 550 nm gradually appeared.[36]

Interestingly, the grafting of ligands **2** and **3** showed a com- pletely different behavior. Indeed, in these cases, an emission enhancement was observed. The mass ratio between ZnO nanoparticles and the organic compounds was optimized to generate the highest emission and was found equal to ZnO:ligand = 2:1. While the emission of ligand **2** is enhanced by a factor up to 500 by the injection of ZnO into the solution, ligand **3** only shows an emission enhancement in the range of 6–10 (Figures 3b,d). Additionally, there is a strong light scat- tering signal appearing in the absorption spectrum of ZnO:**2** indicating the formation of large nanohybrids aggregates while grafting (Figure 3a). Transmission electron microscopy (TEM) analyses confirmed the presence of these tens to hundreds of nanometers large aggregates in solution (Figure S8, Supporting Information). In contrast, grafting of **3** leads to nanohybrids ZnO:**3** highly soluble in chloroform, as validated by DLS/TEM analyses and the absence of any noticeable scattering signal (Figure 3b). In the case of compound **4**, the reference molecule without grafting unit, there is no change in absorption and emission introduced by the presence of ZnO nanoparticles (Figure S6, Supporting Information). This indicates clearly that the optical changes observed for ligands **2** and **3** are directly related to their grafting onto ZnO nanoparticle surfaces. Due to the fact that both ligands **2** and **3** are composed of the same hydroxyoxophosphole grafting unit and only differ by the pres- ence of long alkyl chains in the case of **3**, it can be supposed that the much higher emission enhancement in solution in the case of ZnO:**2** compared to ZnO:**3** is related to the restriction of phenyl ring rotation through the interactions between nanohy- brids inside the large aggregates.

In order to deeper understand the grafting process and the induction of strong AIE effect, the time evolution of the lumi- nescence spectra was studied for the nanohybrids ZnO:**2** and ZnO:**3** right after injection of the ZnO nanoparticles in solu- tion. Simultaneously, the time evolution of their absorption spectra was recorded at 600 nm, i.e., at a wavelength without ligand absorption but well located to measure the optical signal related to light scattering upon aggregates formation (**Figure 4**).

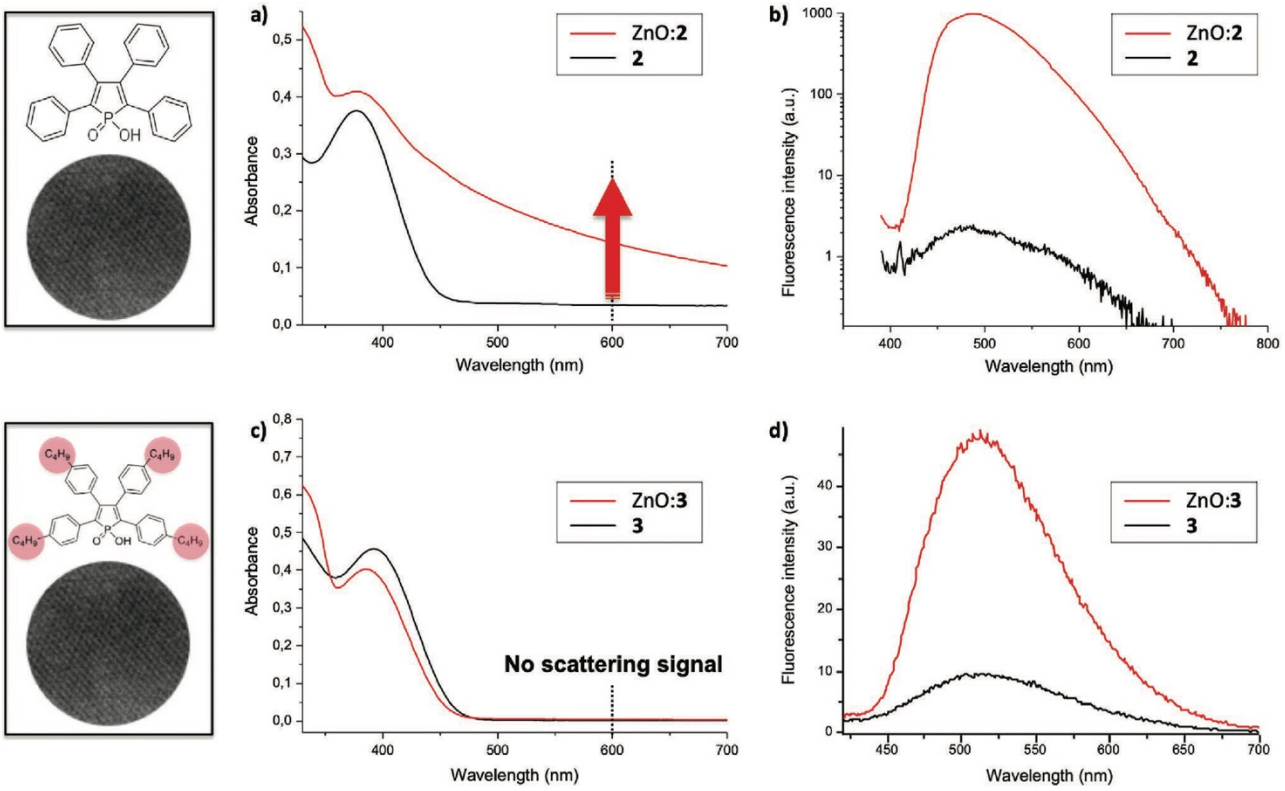

Figure 3. Top: absorption spectra (a) and emission spectra at λ_{ex} = 380 nm (b) of **2** and ZnO:**2** in chloroform solution. Bottom: absorption spectra (c) and emission spectra at λ_{ex} = 380 nm (d) of **3** and ZnO:**3** in chloroform solution.

Dynamic light scattering (DLS) measurements helped to char- acterize the initial ZnO solution, especially to determine that ZnO nanoparticle clusters about 15 nm large were present in this starting solution. Taking into account that the size of the ZnO nanoparticles is 6 nm (±1 nm), there are small clusters composed of few nanoparticles already present in solution before grafting. After injection of ZnO nanoparticles, both nanohybrids ZnO:**2** and ZnO:**3** showed first a weak decrease in light scattering during the first minutes, indicating that the

grafting of the molecules weakly reduced the cluster size of ZnO nanoparticles. In the case of nanohybrids ZnO:**3**, the light scattering signal remained then stable thanks to the solubility of these nanohybrids in solution, whereas the fluorescence inten- sity increased to reach the stable emission enhancement in a factor of 6–10. This moderate increase can be rationalized

on the basis of the chemical modification of the fluorophore upon grafting (loss of the O-H vibrator). Interestingly, in the case of nanohybrids ZnO:**2**, a different behavior with two phases was

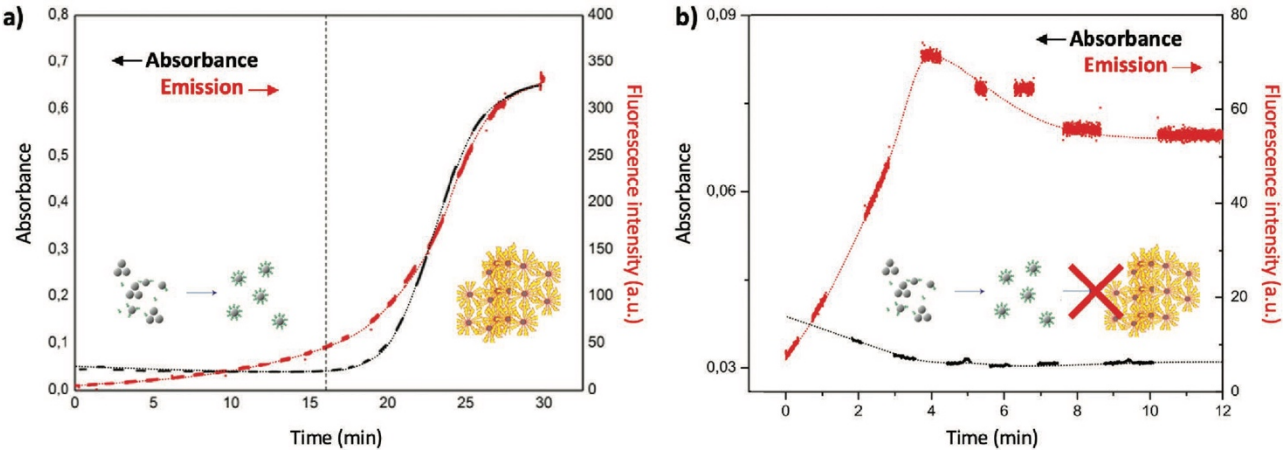

Figure 4. Time resolved absorbance measured at 600 nm (black lines) and fluorescence intensity (red lines) of ZnO:**2** (a) and ZnO:**3** (b) nanohybrids. Zero minute corresponds to the time when ZnO was injected into molecules solution in chloroform.

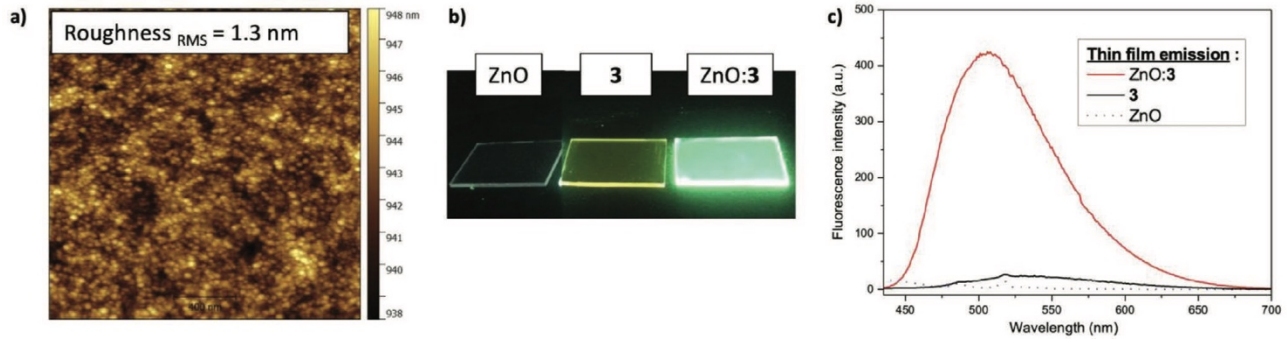

Figure 5. a) AFM image of ZnO:**3** thin film spin-coated on glass substrate. b) Photograph image under UV-light of ZnO, **3** and nanohybrids ZnO:**3** spin-coated thin films. c) Fluorescence spectra of ZnO, **3** and nanohybrids ZnO:**3** thin films at λ_{ex} = 380 nm.

observed. During the first 15 min (see vertical dotted line as eye guide in Figure 4a), the first phase was similar for both nanohybrids as the fluorescence intensity of ZnO:**2** increased by the same typical factor of 8–12. After these 15 min, during the second phase, the scattering signal started to increase strongly and saturated in intensity after 30 min, indicating the formation of ZnO:**2** nanohybrids large aggregates. The corresponding fluorescence intensity increased simultaneously very fast by another factor of 10 with the large aggregates' formation. The later emission enhancement during this second phase can be directly addressed to the restriction of phenyl ring rotation during the large aggregates' formation, i.e., the AIE effect.

2.3. Thin Film Photoluminescence and Electroluminescence

In order to evaluate these novel nanomaterials for lighting applications, we studied the optical properties of ZnO:**2** and ZnO:**3** nanohybrids in thin films. As ZnO:**2** nanohybrids form large aggregates in solution, their solution processing via spin coating onto glass substrates leads to films of poor optical quality. Very high roughness and only partial surface coverage were indeed determined by atomic force microscopy, thus making these nanohybrids non suitable for LED fabrica- tion. In contrast, nanohybrids ZnO:**3**, thanks to their high solubility, allowed the processing of very smooth (RMS rough- ness = 1.3 nm) and closely packed homogeneous layers on glass (**Figure 5**a,b). The layers based on ZnO:**2** are strongly emissive with quantum yields (QY) yield up to 38% as it was expected from the analyses done in solution. Importantly, we found out that also nanohybrids ZnO:**3** formed layers with high emis- sion (Figure 5c) with QY up to 39%, that is strongly increased compared to the free ligand measured in the same conditions ( ) = 0.5%) and more importantly, nearly identical to the emis- sion of ZnO:**2** layers. This result shows clearly that ligand **3**, even grafted onto ZnO nanoparticles, still owns intramolecular rotation of phenyl rings in solution, but processing into thin films definitely freezes phenyl rotations via intermolecular interactions and thus generates strong AIE effect.

While ZnO:**2** films were not suitable for device application due to their poor quality, thanks to the high optical quality of nanohybrids ZnO:**3** thin films, the electroluminescent proper- ties of this material were studied as light-emitting layer in simple

LED structures. The device structure (Figure S9, Supporting Information) consists of ITO/CuPc/HTL/ ZnO:**3**/mCP/Alq_3/LiF/ Al with CuPc as hole injection layer and mCP as hole blocking layer to avoid emission from Alq_3. The hole transport layer (HTL) is a 20 nm thick film of polyvinylcarbazole used to reduce the leakage current within the device. The emitting layer ZnO:**3** is solution-processed on the stack from concentrated nanohy- brids solution (see ESI for details on LED fabrication). The cur- rent density–voltage–luminance (*J–V–L*) curves of the diode (**Figure 6**a) shows a threshold voltage near 4 V with a maximum emission at 90 cd m^{-2} for a current density of 100 mA cm^{-2}. Inset shows two photograph images of the diode working at 30 and 50 mA cm^{-2}, respectively, having homogeneous emission over the whole emitting surface (0.28 cm^2). The electroluminescence spectrum corresponds to the photoluminescence spectrum of nanohybrid ZnO:**3** (maximum at 514 nm) proving that the emis- sion comes from the nanohybrid layer (Figure 6b). These results show that this new class of nanohybrid material is able to act as emissive layer in solution-processed LED devices, even though the moderate luminance and its saturation at high current densi- ties deserve optimizations in future work.

3. Conclusion

To summary, novel fluorescent nanohybrids, based on -extended hydroxyoxophosphole ligands grafted onto ZnO surface, were designed and studied. Furthermore, the restric- tion of the intramolecular motions of the organic fluorophore, through either aggregates' formation in solution or processing into thin films, is found to form highly emissive materials due to a strong AIE effect. Theoretical calculations and XPS anal- ysis show that electronic coupling between the ligands and the ZnO nanoparticles occurs leading to partial charge transfer to the ligand from the ZnO core. Preliminary results on the use of these nanohybrids as solution-processed emissive layers for lighting applications indicate high quantum efficiencies in the thin films allowing electroluminescence. Future work will explore the potential of these nanohybrids using more efficient charge transport layers together with multicolor highly emis- sive graftable molecules leading to major advances compared to pure organic materials or inorganic nanoparticles for lighting devices or optical detections at nanoscale.

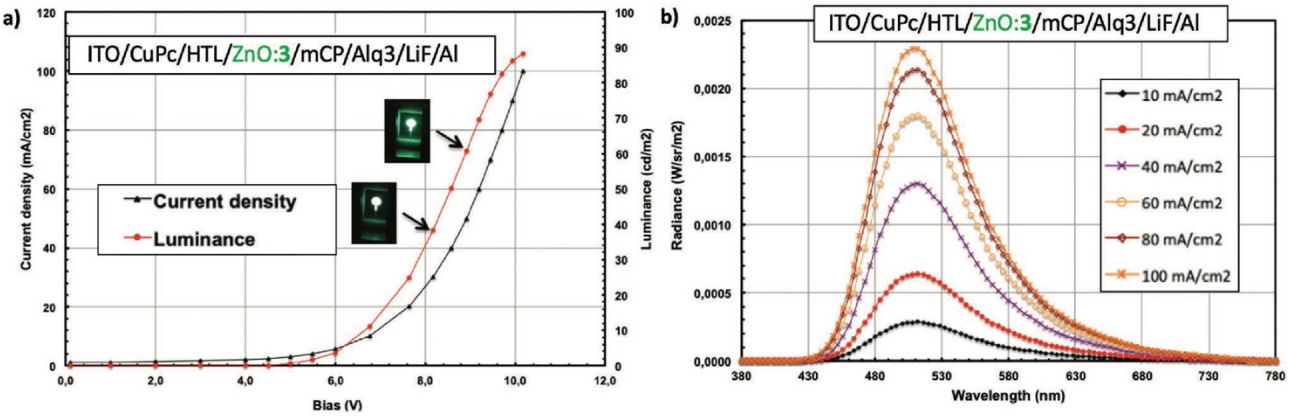

Figure 6. a) Electroluminescent *J–V–L* curves of the light emitting diodes (LEDs) devices. b) Radiance spectra of the LED devices as a function of current density.

4. Experimental Section

All experiments were performed under an atmosphere of dry argon using standard Schlenk techniques. Commercially available reagents were used as received without further purification. Solvents were freshly purified using MBRAUN SPS-800 drying columns. Separations were performed by gravity column chromatography on basic alumina (Aldrich, Type 5016A, 150 mesh, 58 Å) or silica gel (Merck Geduran 60, 0.063–0.200 mm). ^{1}H, ^{13}C, and ^{31}P NMR spectra were recorded on Bruker AV III 300 and 400 MHz NMR spectrometers equipped with BBO or BBFO probeheads. Assignment of proton and carbon atoms is based on COSY, NOESY, edited-HSQC, and HMBC experiments. ^{1}H and ^{13}C NMR chemical shifts were reported in parts per million (ppm) using residual solvent signal as reference. High-resolution mass spectra were obtained on a Varian MAT 311 or ZabSpec TOF Micromass instrument at CRMPO (Scanmat, UMS 2001). UV-Visible spectra were recorded at room temperature on a VARIAN Cary 5000 spectrophotometer. The UV-Vis emission and excitation spectra measurements were recorded on a FL 920 Edimburgh Instrument equipped with a Hamamatsu R5509-73 photomultiplier for the NIR domain (300-1700 nm) and corrected for the response of the photomultiplier. QY in solution were calculated relative to quinine sulfate (H_2SO_4, 0.1 m), $\rangle_{ref} = 0.55$. Detailed syntheses and NMR characterizations of organic compounds are given in Supporting Information.

Supporting Information

Supporting Information is available from the Wiley Online Library or from the author.

Acknowledgements

This work is supported by the Ministère de la Recherche et de l'Enseignement Supérieur, the CNRS, the Région Bretagne (ARED grant to NL), the French National Research Agency (ANR Fluohyb ANR-17-CE09-0020) and the SATT Sud-Est. The authors thank T. Roisnel (CDifX, ISCR) for X-ray diffraction analysis and A.Ranguis (CINaM) for AFM measurements. A.M. acknowledges MUR for project PON04a2 00490 M2M Netergit and PRACE for awarding access to Marconi KNL at CINECA, Italy, through project PROVING-IL (2019204911).

Conflict of Interest

The authors declare no conflict of interest.

Data Availability Statement

Research data are not shared.

Keywords

hybrid materials, AIE, fluorescence, nanoparticles, hydroxyoxoposphole

Received: July 28, 2021 Published online:

[1] W. Yao, Q. Tian, W. Wu, *Adv. Opt. Mater.* **2019**, *7*, 1801171.
[2] E. Thimsen, B. Sadtler, M. Y. Berezin, *Shortwave-infrared (SWIR) Emitters for Biological Imaging: A Review of Challenges and Opportunities*, Vol. *6*, Walter de Gruyter GmbH, Berlin **2017**, pp. 1043–1054.
[3] J. Song, J. Qu, M. T. Swihart, P. N. Prasad, *Nanomedicine* **2016**, *12*, 771. [4] B. S. Mashford, M. Stevenson, Z. Popovic, C. Hamilton, Z. Zhou,

C. Breen, J. Steckel, V. Bulovic, M. Bawendi, S. Coe-Sullivan, P. T. Kazlas, *Nat. Photonics* **2013**, *7*, 407.

[5] D. I. Son, B. W. Kwon, D. H. Park, W.-S. Seo, Y. Yi, B. Angadi, C.-L. Lee, W. K. Choi, *Nat. Nanotechnol.* **2012**, *7*, 465.

[6] U. Resch-Genger, M. Grabolle, S. Cavaliere-Jaricot, R. Nitschke, T. Nann, *Nat. Methods* **2008**, *5*, 763.

[7] Y.-T. Tsai, K.-P. Tseng, Y.-F. Chen, C.-C. Wu, G.-L. Fan, K.-T. Wong, G. Wantz, L. Hirsch, G. Raffy, A. Del Guerzo, D. M. Bassani, *ACS Nano* **2016**, *10*, 998.

[8] E. Genin, Z. Gao, J. A. Varela, J. Daniel, T. Bsaibess, I. Gosse, L. Groc, L. Cognet, M. Blanchard-Desce, *Adv. Mater.* **2014**, *26*, 2258. [9] D. Kim, K. Jeong, J. E. Kwon, H. Park, S. Lee, S. Kim, S. Y. Park, *Nat.Commun.* **2019**, *10*, 3089.

[10] S. Kühn, U. Håkanson, L. Rogobete, V. Sandoghdar, *Phys. Rev. Lett.* **2006**, *97*, 017402.

[11] F. Tam, G. P. Goodrich, B. R. Johnson, N. J. Halas, *Nano Lett..* **2007**, *7*, 496.

[12] X. Cai, R. M. Adhikari, K. C. Anyaogu, S. S. Palayangoda, L. A. Estrada, K. De Puran, D. C. Neckers, *J. Am. Chem. Soc.* **2009**, *131*, 1648.

[13] U. Jabeen, T. Adhikari, S. M. Shah, S. U. Khan, D. Pathak, J. M. Nunzi, *Opt. Mater.* **2018**, *83*, 165.

[14] Y. Hong, J. W. Y. Lam, B. Z. Tang, *Chem. Commun.* **2009**, 4332.

[15] Z. Zhao, H. Zhang, J. W. Y. Lam, B. Z. Tang, *Angew. Chem., Int. Ed.* **2020**, *59*, 9888.

[16] F. Würthner, T. E. Kaiser, C. R. Saha-Möller, *Angew. Chem., Int. Ed.* **2011**, *50*, 3376.

[17] J. Shi, L. E. Aguilar Suarez, S.-J. Yoon, S. Varghese, C. Serpa, S. Y. Park, L. Lüer, D. Roca-Sanjuán, B. Milián-Medina, J. Gierschner, *J. Phys. Chem. C* **2017**, *121*, 23166.

[18] T. Zheng, J.-L. Xu, X.-J. Wang, J. Zhang, X. Jiao, T. Wang, D. Chen, *Chem. Commun.* **2016**, *52*, 6922.

[19] C. Li, X. Liu, M. Yuan, J. Li, Y. Guo, J. Xu, M. Zhu, J. Lv, H. Liu, Y. Li, *Langmuir* **2007**, *23*, 6754.

[20] P. Kumar De, D. C. Neckers, *Photochem. Photobiol. Sci.* **2013**, *12*, 363.

[21] F. Bu, E. Wang, Q. Peng, R. Hu, A. Qin, Z. Zhao, B. Z. Tang, *Chem. - Eur. J.* **2015**, *21*, 4440.

[22] M. P. Duffy, W. Delaunay, P.-A. Bouit, M. Hissler, *Chem. Soc. Rev.* **2016**, *45*, 5296.

[23] Y. Ren, T. Baumgartner, *Dalton Trans.* **2012**, *41*, 7792.

[24] K. Shiraishi, T. Kashiwabara, T. Sanji, M. Tanaka, *New J. Chem.* **2009**, *33*, 1680.

[25] A. Fukazawa, Y. Ichihashi, S. Yamaguchi, *New J. Chem.* **2010**, *34*, 1537.

[26] F. Riobé, R. Szűcs, P.-A. Bouit, D. Tondelier, B. Geffroy, F. Aparicio, J. Buendía, L. Sánchez, R. Réau, L. Nyulászi, M. Hissler, *Chem. - Eur. J.* **2015**, *21*, 6547.

[27] P. Bolle, Y. Chéret, C. Roiland, L. Sanguinet, E. Faulques, H. Serier- Brault, P.-A. Bouit, M. Hissler, R. Dessapt, *Chem. - Asian J.* **2019**, *14*, 1642.

[28] A. Kira, Y. Shibano, S. Kang, H. Hayashi, T. Umeyama, Y. Matano, H. Imahori, *Chem. Lett.* **2010**, *39*, 448.

[29] L. D. Freedman, B. R. Ezzel, R. N. Jenkins, R. M. Harris, *Phosphorus* **1974**, *4*, 199.

[30] J. Rabah, A. Escola, O. Jeannin, P.-A. Bouit, M. Hissler, F. Camerel, *ChemPlusChem* **2020**, *85*, 79.

[31] B. Zhang, T. Kong, W. Xu, R. Su, Y. Gao, G. Cheng, *Langmuir* **2010**, *26*, 4514.

[32] M. Estruga, C. Domingo, J. A. Ayllón, *J. Mater. Chem.* **2011**, *21*, 4408.

[33] D. Liu, W. Wu, Y. Qiu, S. Yang, S. Xiao, Q. Q. Wang, L. Ding, J. Wang, *Langmuir* **2008**, *24*, 5052.

[34] Q. Bao, X. Liu, Y. Xia, F. Gao, L.-D. Kauffmann, O. Margeat, J. Ackermann, M. Fahlman, *J. Mater. Chem. A* **2014**, *2*, 17676.

[35] C. Martini, G. Poize, D. Ferry, D. Kanehira, N. Yoshimoto, J. Ackermann, F. Fages, *ChemPhysChem* **2009**, *10*, 2465.

[36] Y. Gong, T. Andelman, G. F. Neumark, S. O'Brien, I. L. Kuskovsky, *Nanoscale Res. Lett.* **2007**, *2*, 297.